

---

# The frustrated Heisenberg antiferromagnet on the honeycomb lattice: $J_1$ - $J_2$ model

P. H. Y. LI<sup>1</sup>, R. F. BISHOP<sup>1</sup>, D. J. J. FARNELL<sup>2</sup> and C. E. CAMPBELL<sup>3</sup>

<sup>1</sup> *School of Physics & Astronomy, Schuster Building, The University of Manchester, Manchester M13 9PL, UK*

<sup>2</sup> *Division of Mathematics, Faculty of Advanced Technology, University of Glamorgan, Pontypridd CF37 1DL, UK*

<sup>3</sup> *School of Physics & Astronomy, University of Minnesota, 116 Church St. SE, Minneapolis, MN 55455, USA*

PACS 75.10.Jm – Quantised spin models

PACS 75.50.Ee – Antiferromagnetics

**Abstract** – We study the ground-state (gs) phase diagram of the frustrated spin- $\frac{1}{2}$   $J_1$ - $J_2$  antiferromagnet with  $J_2 = \kappa J_1 > 0$  ( $J_1 > 0$ ) on the honeycomb lattice, using the coupled-cluster method. We present results for the ground-state energy, magnetic order parameter and plaquette valence-bond crystal (PVBC) susceptibility. We find a paramagnetic PVBC phase for  $\kappa_{c_1} < \kappa < \kappa_{c_2}$ , where  $\kappa_{c_1} \approx 0.207 \pm 0.003$  and  $\kappa_{c_2} \approx 0.385 \pm 0.010$ . The transition at  $\kappa_{c_1}$  to the Néel phase seems to be a continuous deconfined transition (although we cannot exclude a very narrow intermediate phase in the range  $0.21 \lesssim \kappa \lesssim 0.24$ ), while that at  $\kappa_{c_2}$  is of first-order type to another quasiclassical antiferromagnetic phase that occurs in the classical version of the model only at the isolated and highly degenerate critical point  $\kappa = \frac{1}{2}$ . The spiral phases that are present classically for all values  $\kappa > \frac{1}{6}$  are absent for all  $\kappa \lesssim 1$ .

Two-dimensional (2D) frustrated quantum spin-lattice systems have become of huge interest both theoretically and experimentally [1–3]. Attention has particularly focussed on the rich panoply of (zero-temperature,  $T = 0$ ) quantum phase transitions that they exhibit [3, 4]. Without thermal fluctuations the transitions are driven solely by the interplay of quantum fluctuations and any frustration due to inherent competition between the interactions. Such frustration can arise either dynamically or geometrically. A prototypical example of the former is the well-studied  $J_1$ - $J_2$  Heisenberg antiferromagnet (HAFM) on the bipartite square lattice (see, e.g., Refs. [5–7] and references cited therein), where nearest-neighbour (NN) spins interact via a Heisenberg interaction with strength parameter  $J_1 > 0$ , which competes with a Heisenberg interaction with strength parameter  $J_2 > 0$  between next-nearest neighbour (NNN) pairs. Similar prototypical models exhibiting geometrical frustration are the pure NN HAFMs on the triangular [8] and kagome lattices [9]. For either form of frustration special interest then centres on the possible appearance of novel quantum ground-state (gs) phases without the long-range order (LRO) that typifies the classical gs phases of the corresponding models taken in the limit  $s \rightarrow \infty$  of the spin quantum number  $s$  of the lattice spins. Examples include various valence-bond crystalline

solid phases and spin-liquid phases.

Quantum fluctuations tend to be largest for the smallest values of  $s$ , for lower dimensionality  $D$  of the lattice, and for the smallest coordination of the lattice. Thus, for spin- $\frac{1}{2}$  models in  $D = 2$ , the honeycomb lattice plays a special role. Frustration is easily incorporated via competing NNN and maybe also next-next-nearest-neighbour (NNNN) bonds. Such models and their experimental realisations have been much studied in recent years [10–16]. Additional interest has also sprung from the recent synthesis of graphene monolayers and other magnetic materials with a honeycomb structure. Theoretical interest was spurred by the discovery of a spin-liquid phase in the exactly solvable Kitaev model [17], in which spin- $\frac{1}{2}$  particles reside on a honeycomb lattice. Hubbard models on the honeycomb lattice may also describe many of the relevant physical properties of graphene. For example, evidence has been found [18] that quantum fluctuations are sufficiently strong to establish an insulating spin-liquid phase between the nonmagnetic metallic phase and the antiferromagnetic (AFM) Mott insulator phase, when the Coulomb repulsion parameter  $U$  becomes moderately strong. For large values of  $U$  the latter phase corresponds to the pure HAFM on the bipartite honeycomb lattice, whose gs phase exhibits Néel LRO. However, higher-order terms in the

arXiv:1201.3512v1 [cond-mat.str-el] 17 Jan 2012

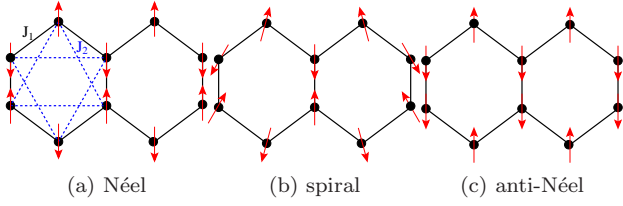


Fig. 1: (Color online) The  $J_1$ - $J_2$  model on the honeycomb lattice (with  $J_1 = 1$ ), showing (a) the Néel, (b) spiral, and (c) anti-Néel states. The arrows represent spins located on lattice sites  $\bullet$ .

$t/U$  expansion of the Hubbard model may lead to frustrating exchange couplings in the corresponding spin-lattice limiting model, in which the HAFM with NN exchange couplings is the leading term in the large- $U$  expansion. There is a growing consensus [10, 11, 13–16] that the frustrated spin- $\frac{1}{2}$  HAFM on the honeycomb lattice undergoes a frustration-induced quantum phase transition to a paramagnetic phase showing no magnetic LRO.

Indirect experimental backup for such theoretical findings comes from recent observations of spin-liquid-like behaviour in the layered compound  $\text{Bi}_3\text{Mn}_4\text{O}_{12}(\text{NO}_3)$  (BMNO) at temperatures below its Curie-Weiss temperature [12]. In BMNO the  $\text{Mn}^{4+}$  ions reside on the sites of (weakly-coupled) honeycomb lattices, but they have spin quantum number  $s = \frac{3}{2}$ . The successful replacement of the  $\text{Mn}^{4+}$  ions in BMNO by  $\text{V}^{4+}$  ions could lead to the realization of a corresponding  $s = \frac{1}{2}$  model on the honeycomb lattice. Other recent realizations of HAFMs on a honeycomb lattice include compounds such as  $\text{Na}_3\text{Cu}_2\text{SbO}_6$  [19] and  $\text{InCu}_{2/3}\text{V}_{1/3}\text{O}_3$  [20], in both of which the  $\text{Cu}^{2+}$  ions in the copper oxide layers form a spin- $\frac{1}{2}$  HAFM on a (distorted) honeycomb lattice. Others include the family of compounds  $\text{BaM}_2(\text{XO}_4)_2$  ( $\text{M}=\text{Co}, \text{Ni}$ ;  $\text{X}=\text{P}, \text{As}$ ) [21], in which the magnetic ions  $\text{M}$  are disposed in weakly-coupled layers where they reside on the sites of a honeycomb lattice. The  $\text{Co}$  ions have spins  $s = \frac{1}{2}$  and the  $\text{Ni}$  ions have spins  $s = 1$ . Finally, recent calculations of the low-dimensional material  $\beta\text{-Cu}_2\text{V}_2\text{O}_7$  [22] show that its magnetic properties can be described in terms of a spin- $\frac{1}{2}$  model on a distorted honeycomb lattice.

In recent papers [23, 24] we have studied the frustrated spin- $\frac{1}{2}$   $J_1$ - $J_2$ - $J_3$  model on the honeycomb lattice [10, 11, 13–16]. Its Hamiltonian is given by

$$H = J_1 \sum_{\langle i,j \rangle} \mathbf{s}_i \cdot \mathbf{s}_j + J_2 \sum_{\langle\langle i,k \rangle\rangle} \mathbf{s}_i \cdot \mathbf{s}_k + J_3 \sum_{\langle\langle\langle i,l \rangle\rangle\rangle} \mathbf{s}_i \cdot \mathbf{s}_l, \quad (1)$$

where index  $i$  runs over all honeycomb lattice sites, and indices  $j$ ,  $k$ , and  $l$  run over all NN, NNN and NNNN sites to  $i$ , respectively, counting each bond once and once only. Each lattice site  $i$  carries a particle with spin  $s = \frac{1}{2}$  and a spin operator  $\mathbf{s}_i = (s_i^x, s_i^y, s_i^z)$ . The lattice and exchange bonds are illustrated in Fig. 1. In earlier work we restricted ourselves to the case where  $J_3 = J_2 > 0$ , but we

dealt both with the AFM case with  $J_1 > 0$  [23] and the ferromagnetic (FM) case with  $J_1 < 0$  [24]. Here we put  $J_3 = 0$ , and hence consider the  $J_1$ - $J_2$  model. We restrict ourselves to the case where both bonds are of AFM type,  $J_1 > 0$  and  $J_2 \equiv \kappa J_1 > 0$ . We henceforth set  $J_1 \equiv 1$ .

The classical ( $s \rightarrow \infty$ ) gs phase diagram of the  $J_1$ - $J_2$ - $J_3$  model on the honeycomb lattice [11, 25] comprises six different phases when  $J_1 > 0$  and the other two bonds,  $J_2$  and  $J_3$ , can take either sign. Three are collinear AFM phases, one is the FM phase, and the other two are different helical phases (and see, e.g., Fig. 2 of Ref. [11]). The AFM phases are the Néel phase (N) shown in Fig. 1(a), the striped (S) phase discussed in our earlier paper [23], and the anti-Néel (aN) phase shown in Fig. 1(c). The S, aN, and N states have, respectively, 1, 2, and all 3 NN spins to a given spin antiparallel to it. Equivalently, if we consider the sites of the honeycomb lattice as comprising a set of parallel sawtooth (or zigzag) chains (in any one of the three equivalent directions), the S state comprises alternating FM chains, while the aN state comprises AFM chains in which NN spins on adjacent chains are parallel. Although there are infinite manifolds of non-coplanar states degenerate in energy with each of the S and aN states at  $T = 0$ , both thermal and quantum fluctuations [11] select the collinear configurations. When  $J_3 > 0$  there is a region in which the spiral state shown in Fig. 1(b) is the stable gs phase. It is characterized by a spiral angle defined so that as we move along the parallel sawtooth chains [drawn in the horizontal direction in Fig. 1(b)] the spin angle increases by  $\pi + \phi$  from one site to the next, and with NN spins on adjacent chains antiparallel. The classical gs energy is minimized for this spiral state when the pitch angle  $\phi = \cos^{-1}[\frac{1}{4}(J_1 - 2J_2)/(J_2 - J_3)]$ , when the energy per spin takes the value,

$$\frac{E_{\text{spiral}}^{\text{cl}}}{N} = \frac{s^2}{2} \left( -J_1 - 2J_2 + J_3 - \frac{1}{4} \frac{(J_1 - 2J_2)^2}{(J_2 - J_3)} \right). \quad (2)$$

We note that as  $\phi \rightarrow 0$  this spiral state becomes the collinear N state with energy per spin,

$$\frac{E_{\text{N}}^{\text{cl}}}{N} = \frac{s^2}{2} (-3J_1 + 6J_2 - 3J_3), \quad (3)$$

and there is a continuous phase transition between these two states on the boundary  $y = \frac{3}{2}x - \frac{1}{4}$ , for  $\frac{1}{6} < x < \frac{1}{2}$ , where  $y \equiv J_3/J_1$  and  $x \equiv J_2/J_1$ . Similarly, as  $\phi \rightarrow \pi$  the spiral state becomes the collinear S state, and there is a continuous phase transition between the two states on the boundary line  $y = \frac{1}{2}x + \frac{1}{4}$ , for  $x > \frac{1}{2}$ . There is a first-order phase transition between the collinear N and S states along the boundary line  $x = \frac{1}{2}$ , for  $y > \frac{1}{2}$ . These three phases (N, S, and spiral) meet at the tricritical point  $(x, y) = (\frac{1}{2}, \frac{1}{2})$ . As  $x \rightarrow \infty$  (for fixed finite  $y$ ), the spiral pitch angle  $\phi \rightarrow \frac{2}{3}\pi$ . In this limit the model becomes two HAFMs on weakly connected interpenetrating triangular lattices, with the usual classical ordering of NN spins oriented at an angle  $\frac{2}{3}\pi$  to each other on each sublattice.

The above three states are the only classical gs phases when  $y > 0$ . For  $y < 0$  the N state persists in a region bounded by the same boundary line as above,  $y = \frac{3}{2}x - \frac{1}{4}$ , for  $-\frac{1}{2} < x < \frac{1}{6}$ , on which it continuously meets a second spiral state, and by the boundary line  $y = -1$ , for  $x < -\frac{1}{2}$ , at which it undergoes a first-order transition to the FM state, which itself is the stable gs phase in the region  $x < -\frac{1}{2}$  and  $y < -1$ . Another collinear AFM state, the aN state shown in Fig. 1(c), with energy per spin,

$$\frac{E_{\text{aN}}^{\text{cl}}}{N} = \frac{s^2}{2}(-J_1 - 2J_2 + 3J_3), \quad (4)$$

becomes the stable gs phase in the region  $x > \frac{1}{2}$ , for  $y < \frac{1}{2}\{x - [x^2 + 2(x - \frac{1}{2})^2]^{1/2}\}$ . On the boundary it undergoes a first-order transition to the spiral state shown in Fig. 1(b). For  $\frac{1}{6} < x < \frac{1}{2}$  the spiral state shown in Fig. 1(b) meets another spiral gs phase on the boundary line  $y = 0$ , at which point there is a first-order transition. The pitch angle of this second spiral phase smoothly approaches the value zero along the above boundary with the N state, and the value  $\pi$  along a second boundary curve that joins the points  $(x, y) = (-\frac{1}{2}, -1)$  and  $(\frac{1}{2}, 0)$ , on which it meets the aN state. Both transitions are continuous ones. This second spiral meets the three collinear states N, aN, and FM at the tetracritical point  $(x, y) = (-\frac{1}{2}, -1)$ .

Henceforth we restrict consideration to the  $J_1$ - $J_2$  model where  $J_3 = 0$  (and  $J_1 \equiv 1$ ). The classical ( $s \rightarrow \infty$ ) model thus has the N state as its gs for  $J_2 < \frac{1}{6}$ , whereas for  $J_2 > \frac{1}{6}$  the gs comprises an infinite family of degenerate coplanar states with spiral order [including that shown in Fig. 1(b)], in which the spiral wave vector can point in any direction [11, 25, 26]. It is found [26] that, to leading order in  $1/s$ , spin wave fluctuations lift this degeneracy by the well-known order-by-disorder mechanism, in favour of specific wave vectors. However, these spiral states for the  $J_1$ - $J_2$  model are expected to be very fragile against quantum fluctuations, and indeed to leading order in  $1/s$  the spin-wave correction to the spiral order parameter has been shown to diverge as  $\log N$ , where  $N$  is the number of lattice sites [26], although it is still possible that higher-order terms in  $1/s$  involving spin-wave interactions could stabilize the spiral order for large enough values of  $s$ . In view of the close proximity of the classical collinear AFM aN state for small values of the NNNN coupling  $J_3$  in the  $J_1$ - $J_2$ - $J_3$  model, it seems very likely that spiral order in the spin- $\frac{1}{2}$   $J_1$ - $J_2$  model might well be totally absent.

To investigate this question further, and more generally to consider the entire  $T = 0$  phase diagram of the  $J_1$ - $J_2$  model, we utilize the coupled cluster method (CCM) [27–29] as in our work for the analogous  $J_1$ - $J_2$ - $J_3$  model with  $J_3 = J_2$  [23]. When used at high orders in the systematic approximation schemes developed for it, the CCM is an accurate approach to tackling a wide variety of quantum spin systems [5–7, 30–36]. In particular, it can accurately locate the quantum critical points (QCPs) in such frustrated systems [6, 7, 31, 32, 34, 36], as well as helping to

determine the nature of the phases involved, including any quantum paramagnetic phases without magnetic order [7].

Since the CCM is a size-extensive method it provides results in the limit  $N \rightarrow \infty$  from the outset. However, it requires us to input a model (or reference) state, with respect to which the quantum correlations may, in principle, be exactly included (and see, e.g., Refs. [5, 37, 38] and references cited therein). We use here the Néel (N), spiral, and anti-Néel (aN) states shown in Fig. 1 as our CCM model states. The CCM then incorporates multi-spin correlations on top of the chosen gs model state  $|\Phi\rangle$  for the correlation operators  $S$  and  $\tilde{S}$  that parametrize the exact gs ket and bra wave functions of the system in the respective exponentiated forms  $|\Psi\rangle = e^S|\Phi\rangle$  and  $\langle\tilde{\Psi}| = \langle\Phi|\tilde{S}e^{-S}$ , where  $\langle\tilde{\Psi}|\Psi\rangle \equiv 1$ . The Schrödinger ket and bra equations are  $H|\Psi\rangle = E|\Psi\rangle$  and  $\langle\tilde{\Psi}|H = E\langle\tilde{\Psi}|$  respectively. The correlation operators are defined as  $S = \sum_{I \neq 0} \mathcal{S}_I C_I^+$  and  $\tilde{S} = 1 + \sum_{I \neq 0} \tilde{\mathcal{S}}_I C_I^-$  respectively. The operators  $C_I^+ \equiv (C_I^-)^\dagger$  and  $C_I^-$  are the creation and destruction operators respectively, where  $C_0^+ \equiv 1$  and  $\langle\Phi|C_I^+ = 0; \forall I \neq 0$ . The set  $\{C_I^+ \equiv s_{j_1}^+ s_{j_2}^+ \cdots s_{j_n}^+\}$ , where  $s_j^+ \equiv s_j^x + i s_j^y$ , forms a complete set of multispin creation operators with respect to the model state  $|\Phi\rangle$  as a generalized vacuum. We then calculate the correlation coefficients  $\{\mathcal{S}_I, \tilde{\mathcal{S}}_I\}$  by minimizing the gs energy expectation value  $\bar{H} \equiv \langle\tilde{\Psi}|H|\Psi\rangle$  with respect to each of them. This yields the coupled sets of equations  $\langle\Phi|C_I^- e^{-S} H e^S |\Phi\rangle = 0$  and  $\langle\Phi|\tilde{S}(e^{-S} H e^S - E)C_I^+ |\Phi\rangle = 0; \forall I \neq 0$ , which are used to calculate the ket- and bra-state correlation coefficients within specific truncation schemes on the retained set  $\{I\}$  described below. It is necessary to use parallel computing routines for high-order computation [37–39].

For the  $s = \frac{1}{2}$  case considered here we use the well-tested localized LSUB $m$  truncation scheme which includes all multi-spin correlations in the CCM correlation operators over all regions on the lattice defined by  $m$  or fewer contiguous lattice sites. The numbers  $N_f$  of such fundamental configurations that are distinct under the symmetries of the lattice and the model state in various LSUB $m$  approximations increases rapidly with the truncation index  $m$ . For example, the highest LSUB $m$  level that we can reach, even with massive parallelization and the use of super-computing resources, is LSUB12, for which  $N_f = 293309$  for the aN state. The raw LSUB $m$  data still need to be extrapolated to the exact  $m \rightarrow \infty$  limit. Although there are no exact extrapolation rules we have a great deal of experience in doing so. Thus, for the gs energy per spin,  $E/N$ , we use (see, e.g., Refs., [6, 7, 31, 32, 34, 38])

$$E(m)/N = a_0 + a_1 m^{-2} + a_2 m^{-4}; \quad (5)$$

while for the magnetic order parameter (sublattice magnetization),  $M$ , we use either the scheme

$$M(m) = b_0 + b_1 m^{-1} + b_2 m^{-2}, \quad (6)$$

for systems showing no or only slight frustration (see, e.g.,

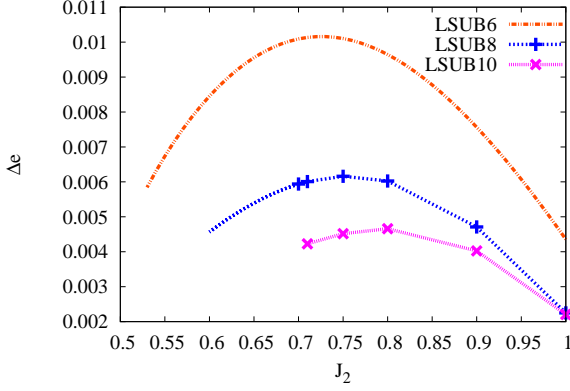


Fig. 2: Difference between the gs energies per spin ( $e \equiv E/N$ ) of the spiral and anti-Néel phases ( $\Delta e \equiv e^{\text{spiral}} - e^{\text{aN}}$ ) versus  $J_2$  for the spin- $\frac{1}{2}$   $J_1$ - $J_2$  honeycomb model ( $J_1 = 1$ ) in LSUB $m$  approximations with  $m = \{6, 8, 10\}$ .

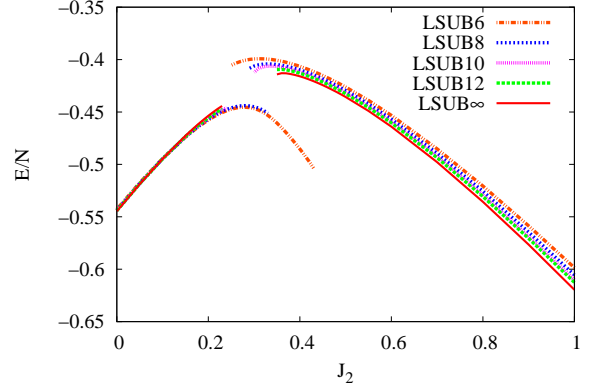


Fig. 3: CCM LSUB $m$  results for the gs energy,  $E/N$ , of the Néel and anti-Néel phases of the spin- $\frac{1}{2}$   $J_1$ - $J_2$  honeycomb model ( $J_1 = 1$ ), with  $m = \{6, 8, 10, 12\}$  and the extrapolated LSUB $\infty$  result using this data set.

Refs. [30, 31]), or the scheme

$$M(m) = c_0 + c_1 m^{-1/2} + b_2 m^{-3/2}, \quad (7)$$

for more strongly frustrated systems or ones showing a gs order-disorder transition (see, e.g., Refs. [6, 7, 34, 36]). Since the hexagon is an important structural element of the honeycomb lattice we perform the extrapolations only for LSUB $m$  data with  $m \geq 6$ .

We show in Fig. 2 the difference in the gs energies of the CCM LSUB $m$  results based on the spiral and aN model states. For the spiral state the pitch angle at a given LSUB $m$  level is chosen to minimize the corresponding estimate for the gs energy. Although the energy differences are small the results for all values of  $m$ , as well as the extrapolated results, show clearly that, as expected from our previous discussion, the spiral state that is the classical gs for all values  $\kappa \equiv J_2/J_1 > 0.5$  gives way to the collinear aN state as the stable gs phase for the spin- $\frac{1}{2}$  model out to much higher values of  $\kappa$ . If a quantum phase transition between the spiral and aN states does exist, Fig. 2 shows that it can occur only at a value  $\kappa > 1$ . Henceforth we concentrate on gs phases other than the spiral phase.

In Fig. 3 we show results for the gs energy per spin,  $E/N$ , using the N and aN states as model states. We observe that each of the energy curves based on a particular model state terminates at some critical value of  $\kappa$  (that itself depends on the LSUB $m$  approximation used), beyond which no real CCM solution can be found. We note that in Fig. 2 results are shown for each LSUB $m$  case down to values of  $\kappa$  at which real solutions based on the spiral model state cease to exist. In all cases the corresponding termination point at a given LSUB $m$  level shown in Fig. 3 for aN model state is lower than that for the equivalent spiral model state case. Such terminations of the CCM solutions are well understood [29, 35]. They are simply manifestations of the quantum phase transitions in the real system, and may thus be used to estimate the positions of the

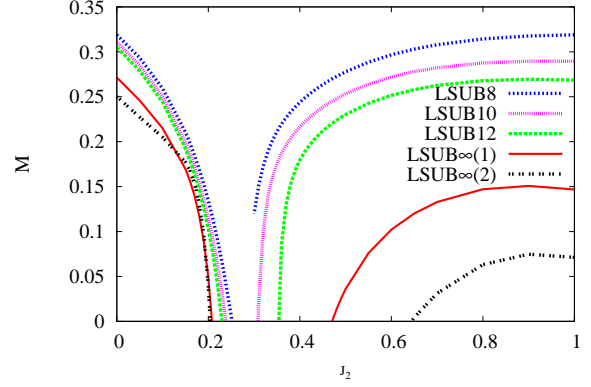


Fig. 4: CCM LSUB $m$  results for the gs order parameter,  $M$ , of the Néel and anti-Néel phases of the spin- $\frac{1}{2}$   $J_1$ - $J_2$  honeycomb model ( $J_1 = 1$ ), with  $m = \{8, 10, 12\}$ , and the extrapolated LSUB $\infty$ (1) and LSUB $\infty$ (2) results using this data set and Eqs. (6) and (7) respectively.

corresponding QCPs [29], although we do not do so here since we have more accurate criteria available as discussed below. We note, however, that as is usually the case, the CCM LSUB $m$  results for finite  $m$  values for both the N and aN phases shown in Fig. 3 extend beyond the corresponding LSUB $\infty$  transition points. For large values of  $m$  each LSUB $m$  transition point is quite close to the actual QCP where that phase ends. For example, the LSUB12 termination points shown in Fig. 3 are at  $\kappa_t^{\text{N}} \approx 0.23$  for the N state and  $\kappa_t^{\text{aN}} \approx 0.35$  for the aN state. The CCM results show a clear intermediate regime in which neither of the quasiclassical AFM states (N or aN) is stable.

We now discuss the magnetic order parameter,  $M$ , in order to investigate the stability of quasiclassical magnetic LRO. Our CCM results for  $M$  are shown in Fig. 4. The extrapolated Néel order parameter goes to zero at a value  $\kappa_{c_1}$  that is very insensitive both to which extrapolation scheme

is used of Eqs. (6) or (7), and to whether or not we include the LSUB6 data point in the extrapolations. Our best estimate is  $\kappa_{c_1} \approx 0.207 \pm 0.003$ . This value can be considered as our first CCM estimate of the corresponding QCP of the model. It is in reasonable agreement with, but much more precise than, similar estimates for  $\kappa_{c_1}$  of about 0.17-0.22 from an exact diagonalization (ED) approach [16], about 0.2 from an alternative ED approach [13], about 0.2 from a Schwinger boson approach [10], and about 0.13-0.17 from a pseudo-fermion functional renormalization group approach [15], but in substantial disagreement with a recent variational Monte Carlo (VMC) estimate of about 0.08 [40]. As the authors admit, the VMC study seems to substantially underestimate the QCP  $\kappa_{c_1}$  at which Néel order disappears. As expected, our own estimate shows that, as usual, quantum fluctuations preserve the collinear Néel order to stronger frustrations than the corresponding classical transition to noncollinear spiral order at  $\kappa_{c_1} = \frac{1}{6}$ .

By contrast with the situation at the lower QCP at  $\kappa_{c_1}$ , Fig. 4 shows that the corresponding QCP at  $\kappa_{c_2}$  at which the anti-Néel order vanishes is considerably more difficult to estimate from the extrapolated CCM LSUB $m$  values, with estimates that range from 0.47 to 0.64. We find a much more accurate estimate for  $\kappa_{c_2}$  below. Nevertheless it is clear already that a new quantum phase exists in the range  $\kappa_{c_1} < \kappa < \kappa_{c_2}$ . It is also clear that, as suggested above, the two QCPs are very close to the corresponding CCM termination points seen in Fig. 3. In our previous work on the spin- $\frac{1}{2}$   $J_1$ - $J_2$ - $J_3$  model on the honeycomb lattice [23] with  $J_1 = 1$ , we found strong evidence for a nonmagnetic plaquette valence-bond crystal (PVBC) phase along the line  $J_3 = J_2$  between the two quasiclassical AFM phases, namely the Néel (N) and striped (S) phases. It seems likely that the corresponding phase in the present  $J_3 = 0$  case, which now intervenes between the N and aN phases, might also be the same PVBC phase.

In order to investigate the possibility of a PBVC phase we consider a generalized susceptibility  $\chi_F$  that describes the response of the system to a “field” operator  $F$  (see, e.g., Ref. [7]). A field term  $F = \delta \hat{O}$  is added to the Hamiltonian (1), where  $\hat{O}$  is an operator which corresponds here to the possible PVBC order illustrated in Fig. 5, and which thus breaks the translational symmetry of  $H$ . The energy per site  $E(\delta)/N = e(\delta)$  is then calculated in the CCM for the perturbed Hamiltonian  $H + F$ , using both the N and aN model states. The susceptibility is defined as  $\chi_F \equiv -(\partial^2 e(\delta))/(\partial \delta^2)|_{\delta=0}$ . Clearly, the gs phase becomes unstable against the perturbation  $F$  when  $\chi_F^{-1}$  becomes zero. As in Ref. [23] we use the extrapolation scheme  $\chi_F^{-1}(m) = d_0 + d_1 m^{-2} + d_2 m^{-4}$ .

Our CCM results for  $\chi_F^{-1}$  are shown in Fig. 5. The number of LSUB12 fundamental configurations for the plaquette susceptibility for the aN state is  $N_f = 877315$ . The extrapolated inverse susceptibility vanishes on the Néel side at  $\kappa \approx 0.24 \pm 0.01$  and on the anti-Néel side at  $\kappa \approx 0.385 \pm 0.010$ . The shape of the CCM curves where  $\chi_F^{-1} \rightarrow 0$  on the Néel side is strongly suggestive of a contin-

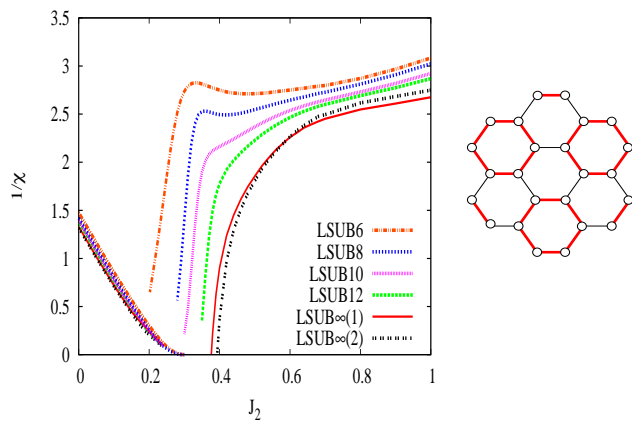


Fig. 5: (Color online) Left: CCM LSUB $m$  results for the inverse plaquette susceptibility,  $1/\chi$ , of the Néel and anti-Néel phases of the spin- $\frac{1}{2}$   $J_1$ - $J_2$  honeycomb model ( $J_1 = 1$ ) with  $m = \{6, 8, 10, 12\}$ , and the extrapolated results LSUB $\infty$ (1) using  $m = \{6, 8, 10, 12\}$  and LSUB $\infty$ (2) using  $m = \{8, 10, 12\}$  (see text). Right: The fields  $F = \delta \hat{O}$  for the plaquette susceptibility  $\chi$ . Thick (red) and thin (black) lines correspond respectively to strengthened and weakened NN exchange couplings, where  $\hat{O} = \sum_{\langle i,j \rangle} a_{ij} \mathbf{s}_i \cdot \mathbf{s}_j$ , and the sum runs over all NN bonds, with  $a_{ij} = +1$  and  $-1$  for thick (red) and thin (black) lines respectively.

uous transition there, just as we found for the corresponding  $J_1$ - $J_2$ - $J_3$  model [23]. The shallow slope of the  $\chi_F^{-1}$  curves there makes it difficult to estimate accurately the point where it vanishes. Nevertheless it is certainly consistent with the much more accurate value we obtained for  $\kappa_{c_1}$  above from the point where the Néel order parameter  $M$  vanishes. On the other hand we cannot exclude the possibility of the transition between the Néel and PVBC states occurring via an intermediate phase that exists in the region  $\kappa_{c_1} < \kappa \lesssim 0.24$ . Just such an intermediate (resonating valence bond spin-liquid) state has been discussed in Ref. [11]. By contrast, the shape of the CCM curves for  $\chi_F^{-1}$  on the anti-Néel side are much more indicative of a first-order transition, and the point where  $\chi_F^{-1} \rightarrow 0$  on that side gives us our best estimate for  $\kappa_{c_2} \approx 0.385 \pm 0.010$ . Again, this value is in good agreement with, but much more accurate than, estimates of about 0.35-0.4 from two different ED studies [13,16]. On both the N and aN sides it seems very likely that the PVBC phase occurs at, or very close to, the QCPs where the quasiclassical magnetic LRO in the N and aN phases vanishes. Since the N and PVBC phases break different symmetries, and our CCM results show that they appear to meet at  $\kappa_{c_1} \approx 0.21$  at a continuous transition, they support the deconfinement scenario there. The possibility of deconfined quantum criticality for the frustrated honeycomb HAFM was pointed out in Ref. [1], and supporting evidence for the  $J_1$ - $J_2$ - $J_3$  model

has also been found both by us [23] and by others [16].

We have studied the influence of quantum spin fluctuations on the gs properties of the spin- $\frac{1}{2}$   $J_1$ - $J_2$  HAFM ( $J_1 > 0, \kappa \equiv J_2/J_1$ ) on the honeycomb lattice. We find a paramagnetic PVBC phase in the regime  $\kappa_{c_1} < \kappa < \kappa_{c_2}$ , where  $\kappa_{c_1} \approx 0.207 \pm 0.003$  and  $\kappa_{c_2} \approx 0.385 \pm 0.010$ . The transition at  $\kappa_{c_1}$  to the Néel phase appears to be a continuous transition of the deconfinement variety, while that at  $\kappa_{c_2}$  is of first-order type to an anti-Néel-ordered AFM phase that does not occur in the classical version of the model except at the critical point  $\kappa = \frac{1}{2}$ . Our results indicate that the spiral phases that exist classically for all values  $\kappa > \frac{1}{6}$  are absent for all values  $\kappa \lesssim 1$ , but may exist for larger values. To investigate this and other aspects of the model further we shall present results in a future paper on the phase diagram of the extended  $J_1$ - $J_2$ - $J_3$  model, using the same CCM techniques.

We thank the University of Minnesota Supercomputing Institute for the grant of supercomputing facilities.

#### REFERENCES

- [1] SENTHIL T., VISHWANATH A., BALENTS L., SACHDEV S. and FISHER M. P. A., *Science*, **303** (2004) 1490.
- [2] MOESSNER R. and RAMIREZ A. P., *Phys. Today*, **59** (February 2006) 24.
- [3] *Quantum Magnetism*, edited by SCHOLLWÖCK U., RICHTER J., FARNELL D. J. J. and BISHOP R. F., *Lecture Notes in Physics*, Vol. **645** (Springer-Verlag, Berlin) 2004.
- [4] *Quantum Phase Transitions*, SACHDEV S., (Cambridge Univ. Press, Cambridge) 1999.
- [5] BISHOP R. F., FARNELL D. J. J. and PARKINSON J. B., *Phys. Rev. B*, **58** (1998) 6394.
- [6] BISHOP R. F., LI P. H. Y., DARRADI R., SCHULENBURG J. and RICHTER J., *Phys. Rev. B*, **78** (2008) 054412.
- [7] DARRADI R., DERZHKO O., ZINKE R., SCHULENBURG J., KRÜGER S. E. and RICHTER J., *Phys. Rev. B*, **78** (2008) 214415.
- [8] BERNU B., LHUILLIER C. and PIERRE L., *Phys. Rev. Lett.*, **69** (1992) 2590.
- [9] SCHNYDER A. P., STARYKH O. A. and L. BALENTS, *Phys. Rev. B*, **78** (2008) 174420.
- [10] MATTSSON A., FRÖJDH P. and EINARSSON T., *Phys. Rev. B*, **49** (1994) 3997.
- [11] FOUET J. B., SINDZINGRE P. and LHUILLIER C., *Eur. Phys. J. B*, **20** (2001) 241.
- [12] OKUBO S., ELMASRY F., ZHANG W., FUJISAWA M., SAKURAI T., OHTA H., AZUMA M., SUMIRNOVA O. A. and KUMADA N., *J. Phys.: Conf. Series*, **200** (2010) 022042.
- [13] MOSADEQ H., SHAHBAZI F. and JAFARI S. A., *J. Phys.: Condens. Matter*, **23** (2011) 226006.
- [14] CABRA D. C., LAMAS C. A. and ROSALES H. D., *Phys. Rev. B*, **83** (2011) 094506.
- [15] REUTHER J., ABANIN D. A. and THOMALE R., *Phys. Rev. B*, **84** (2011) 014417.
- [16] ALBUQUERQUE A. F., SCHWANDT D., HETÉNYI B., CAPPONI S., MAMBRINI M. and LÄUCHLI A. M., *Phys. Rev. B*, **84** (2011) 024406.
- [17] KITAEV A., *Ann. Phys. (N.Y.)*, **321** (2006) 2.
- [18] MENG Z. Y., LANG T. C., WESSEL S., ASSAAD F. F. and MURAMATSU A., *Nature*, **464** (2010) 847.
- [19] MIURA Y., HIARI R., KOBAYASHI Y. and SATO M., *J. Phys. Soc. Jpn.*, **75** (2006) 084707.
- [20] KATAEV V., MÖLLER A., LÖW U., JUNG W., SCHITNER N., KRIENER M. and FREIMUTH A., *J. Magn. Magn. Mater.*, **290-291** (2005) 310.
- [21] REGNAULT L. P. and ROSSAT-MIGNOD J., in *Phase Transitions in Quasi-Two-Dimensional Planar Magnets*, edited by DE JONGH L. J. (Kluwer Academic Publishers) 1990, p. 271.
- [22] TSIRLIN A. A., JANSON O. and ROSNER H., *Phys. Rev. B*, **82** (2010) 144416.
- [23] FARNELL D. J. J., BISHOP R. F., LI P. H. Y., RICHTER J. and CAMPBELL C. E., *Phys. Rev. B*, **84** (2011) 012403.
- [24] LI P. H. Y., BISHOP R. F., FARNELL D. J. J., RICHTER J. and CAMPBELL C. E., *preprint arXiv:1109.6229*, (2011).
- [25] RASTELLI E., TASSI A. and REATTO L., *Physica*, **97B** (1979) 1.
- [26] MULDER A., GANESH R., CAPRIOTTI L. and PARAMAKANTI A., *Phys. Rev. B*, **81** (2010) 214419.
- [27] BISHOP R. F., *Theor. Chim. Acta*, **80** (1991) 95.
- [28] BISHOP R. F., in *Microscopic Quantum Many-Body Theories and Their Applications*, edited by NAVARRO J. and POLLS A., Vol. **510** of *Lecture Notes in Physics* (Springer-Verlag, Berlin) 1998, p.1.
- [29] FARNELL D. J. J. and BISHOP R. F., in *Quantum Magnetism*, edited by SCHOLLWÖCK U., RICHTER J., FARNELL D. J. J. and BISHOP R. F., Vol. **645** of *Lecture Notes in Physics* (Springer-Verlag, Berlin) 2004, p.307.
- [30] KRÜGER S. E., RICHTER J., SCHULENBURG J., FARNELL D. J. J. and BISHOP R. F., *Phys. Rev. B*, **61** (2000) 14607.
- [31] DARRADI R., RICHTER J. and FARNELL D. J. J., *Phys. Rev. B*, **72** (2005) 104425.
- [32] SCHMALFUSS D., DARRADI R., RICHTER J., SCHULENBURG J. and IHLE D., *Phys. Rev. Lett.*, **97** (2006) 157201.
- [33] FARNELL D. J. J., RICHTER J., ZINKE R. and BISHOP R. F., *J. Stat. Phys.*, **135** (2009) 175.
- [34] RICHTER J., DARRADI R., SCHULENBURG J., FARNELL D. J. J. and ROSNER H., *Phys. Rev. B*, **81** (2010) 174429.
- [35] BISHOP R. F., LI P. H. Y., FARNELL D. J. J. and CAMPBELL C. E., *Phys. Rev. B*, **82** (2010) 024416.
- [36] REUTHER J., WÖLFLE P., DARRADI R., BREINIG W., ARLEGO M. and RICHTER J., *Phys. Rev. B*, **83** (2011) 064416.
- [37] ZENG C., FARNELL D. J. J. and BISHOP R. F., *J. Stat. Phys.*, **90** (1998) 327.
- [38] BISHOP R. F., FARNELL D. J. J., KRÜGER S.E., PARKINSON J. B., RICHTER J. and ZENG C., *J. Phys.: Condens. Matter*, **12** (2000) 6887.
- [39] We use the program package CCCM of D. J. J. Farnell and J. Schulenburg, see <http://www-e.uni-magdeburg.de/jschulen/ccm/index.html>.
- [40] CLARK B. K., ABANIN D. A. and SONDHI S. L., *Phys. Rev. Lett.*, **107** (2011) 087204.